Current Research in Food Science 6 (2023) 100524

Contents lists available at ScienceDirect

Current Research in Food Science

journal homepage: www.sciencedirect.com/journal/current-research-in-food-science

Research on the correlation between three-dimensional morphology and temperature changes in potato slices during drying

Li Sun [a,b,*], Xin Zheng [b], Pengqi Zhang [b], Jianrong Cai [a], Junwen Bai [a]

[a] School of Food and Biological Engineering, Jiangsu University, Zhenjiang, 212013, Jiangsu, PR China
[b] School of Mechanical Engineering, Jiangsu University, Zhenjiang, 212013, Jiangsu, PR China

ARTICLE INFO

Handling Editor: Dr. Maria Corradini

Keywords:
Potato slices
Drying
3D morphology
Temperature field
Correlation analysis

ABSTRACT

Drying is an effective method to reduce potato storage loss. However, potatoes have high porosity with high water content. Shrinkage during drying can lead to folding and cracking of the dried product form. Therefore, this study explored the correlation between the 3D morphology and temperature distribution changes of potato slices during drying, with the aim of providing a reference for the detection of quality changes. An online automatic acquisition device to obtain 3D morphology and temperature information was designed and built. Hot air-drying experiments were conducted on the potato slices. 3D morphology images and temperature images of the potato slices were acquired by 3D and temperature sensors, and the two images were registered using the random sample consensus (RANSAC) algorithm. The region of interest of each image was extracted by algorithms such as threshold segmentation, hole filling and morphological erosion, and the 3D morphology information and temperature information were obtained. The mapping, range and average of each acquisition point were calculated for correlation analysis. Spearman's rank correlation coefficients and Maximum Information Coefficient (MIC) values were selected as measures for the correlation study. The results showed that the Spearman's rank correlation coefficients between average height and average temperature were mostly above 0.7 in absolute value, and the MICs were mostly above 0.9. The average values of the 3D information and temperature information exhibited an extremely strong correlation. This paper gives a new approach to investigate the morphological changes in the drying process by quantifying the relationship between 3D morphology and temperature distribution. This can guide the improvement of potato drying and processing methods.

1. Introduction

China's potato production areas are mainly distributed in the northern one-season crop area, the Central Plains two-season crop area, the southwest one- and two-season mixed crop area, and the southern winter crop area (Zhang, 2021; Liu, 2021). The annual cultivation time and production cycle of potatoes vary considerably depending on the climate, environment and soil of the region, and the maturity period differs accordingly. This means that potatoes are available for a longer period of time throughout the year. In recent years, the consumption of processed potato products such as crisps, French fries, potato flour bread and other snack foods and fast foods has grown rapidly. Around 14% of potatoes undergo further processing each year (Gao et al., 2021). As a result, the demand for specialized and large-scale potato production and processing is gradually growing (Huang et al., 2017).

Potatoes are highly water-active and only maintain good shelf quality in storage for 30 days (Xu et al., 2022). The average loss rate during storage is between 10% and 15% (Luo et al., 2015). Potatoes can turn green, sprout or rot during storage, resulting in a rapid increase in solanine content; this can cause symptoms of food poisoning in humans, leading to food safety issues (Cheng et al., 2020). Drying technology is used extensively in the primary processing of potatoes around the world. By significantly reducing the water content of potatoes, the drying process inhibits the microbial activity inside the potatoes. This effectively reduces storage losses (Feng et al., 2018). However, potatoes have high porosity and a water content of up to 80%. During the drying process, they shrink due to the loss of moisture (Liu, 2020). The stress generated during shrinkage can lead to folding and cracking of the dried product form, resulting in a poor-quality finished product (Md Mahiuddin et al., 2018). Therefore, it is important to investigate the mechanism underlying shrinkage and the process of morphological change that occurs during the hot air-drying process. Such information

* Corresponding author. School of Food and Biological Engineering, Jiangsu University, Zhenjiang 212013, Jiangsu, PR China.
E-mail address: raulsunli@ujs.edu.cn (L. Sun).

https://doi.org/10.1016/j.crfs.2023.100524
Received 28 March 2023; Received in revised form 9 May 2023; Accepted 21 May 2023
Available online 30 May 2023

can guide the improvement of potato drying and processing methods.

Machine vision is an effective method to study material morphological changes. With the gradual failure of two-dimensional (2D) flat information to meet application needs, three-dimensional (3D) visual inspection has become a research hotspot (Wang and Wang, 2010). The methods for 3D information acquisition mainly include the binocular stereo vision method (Yang et al., 2021; Liu et al., 2020; Bernhard et al., 2007), the laser triangulation method (Chen, 2019; Shivangi Kelkar et al., 2011), the structured light 3D imaging method (Jiang et al., 2019; Sepehr Makhsous et al., 2019) and the time-of-flight (TOF) method (Zheng et al., 2016; George et al., 2013; Sun et al., 2021). In recent years, along with an increasing emphasis on agriculture in China, 3D visual inspection has become widely used in the field of agricultural production. Bernhard et al. (2007) used 3D techniques to perform 3D reconstruction as a way to measure the structural parameters of the plant canopy under field conditions. The 3D technique was also used by George et al. (2013) to examine the structure of two types of vegetation growing in Californian grasslands.

Temperature detection has also been used in the agricultural sector for many years. Most studies to date have focused on the examination of a single temperature value (Khan Hammad A et al., 2021; Moore Caitlin E et al., 2021; Wang et al., 2021). However, the information that can be gleaned from a single value is very limited. Therefore, temperature fields reflecting the temperature distribution in space and time have become a research topic of interest. With the continuous development of thermal imaging technology, infrared thermal imagers are now widely used in the field of agriculture. This has led to a gradual increase in research on the role of temperature field detection in agriculture (Anne-Katrin et al., 2019; Colaizzi Paul et al., 2018). The application of temperature fields to the drying analysis is helpful to analyze and understand the material drying process. Cheng (2018) performed a simulation of the temperature field for microwave vacuum drying of potato slices. The process of converting microwave energy into internal energy in potatoes was observed in the form of temperature by solving for the temperature field. Wang et al. (2018) simulated the grain drying process by analyzing the temperature field of the drying equipment and investigated the effect of the working parameters on the drying effect.

The current research on material drying focuses mostly on investigating the influence of drying parameters such as temperature and air speed on the drying effect, so as to obtain the best parameters for drying. However, the deeper intrinsic relationship between the two has not been explored. Thus, hot air-drying tests were conducted for each potato slice to quantify the relationship between shrinkage and temperature distribution due to different drying parameters. In this paper, a registration algorithm was designed for use on images acquired by a 3D sensor and infrared thermal imaging sensor. Correlation analysis of the changes in the 3D morphology and temperature distribution of the potato slices during the drying process was conducted. The drying shrinkage was obtained from the material temperature distribution in order to provide a reference for the detection of quality changes during the material drying process.

2. Materials and methods

2.1. Samples

Fresh potatoes, of the Dutch variety, were purchased from the Kaiyuan supermarket at Jiangsu University and were placed in an indoor environment at 17 °C and 30% relative humidity (RH) for one day. Before the experiment, the potatoes were cleaned of soil, dried, and sliced into slices of 2 mm, 4 mm and 6 mm thickness using a slicer. Slices of uniform thickness were selected, and ring cutters of different diameters were used to cut the centre of each potato slice into a round segment of the required diameter: 25 mm, 30 mm, 35 mm. Then, the surface of each round slice was blotted with absorbent paper to remove any residual juice. Four potato slices were prepared for each experimental group: two for 3D image acquisition, one for temperature information acquisition and the remaining one for weighing.

2.2. Experiment equipment

2.2.1. Drying equipment

A homemade tunnel hot air dryer (Fig. 1) was used for the experiments (Cai et al., 2019). The drying chamber was equipped with temperature and humidity sensors. The temperature sensor was able to detect temperatures in the range of −40 to 120 °C, with an accuracy of ±0.5 °C. The humidity sensor had a detection range of 0–100% RH and an accuracy of ±5% RH. After receiving the data from the temperature and humidity sensors, the control box adjusted the temperature, humidity and wind speed by modulating the drying room, dehumidifier fan, steam humidifier, heating device and centrifugal fan. The temperature and humidity were controlled by means of proportional-integral-derivative (PID) control. The wind speed control was open-loop and could produce wind speeds of up to 13 m/s.

2.2.2. Image acquisition platform

3D information and temperature information were acquired during the drying of potato slices. The 3D information was acquired using a structured light 3D sensor from LMI company, model Gocator 3210. Its XY axis resolution was 0.060–0.090 mm, with a measurement accuracy of ±0.035 mm. The temperature information was acquired using an infrared thermal imaging sensor, model Flir A35. It had a temperature measurement range of −40 to +550 °C and a measurement accuracy of ±5 °C.

During operation, the drying chamber was a high temperature and high humidity environment, which can lead to errors in the sensor detection results. Therefore, 3D and temperature information of the potato slices could not be directly obtained from the drying chamber. Thus, an online automatic acquisition device (Fig. 2) for obtaining 3D and temperature information during the drying process of potato slices was designed. This device consisted of a mechanical structure module, a motion control module and an information acquisition module. It automatically lifted the drying platform containing the potato slices out of the drying chamber and controlled the sensors for automatic acquisition. This reduced the errors and improved the accuracy of the acquisition results.

The external framework dimensions of the online acquisition device were 780 mm × 780 mm × 1465 mm. The device controlled a stepping motor using a programmable logic controller (PLC). The linear motion module converted the rotary motion of the stepping motor into the linear motion of the platform. This enabled the rise and fall of the drying platform. The acquisition of image information was performed by 3D and temperature sensors, which were mounted on a fixed plate on the top of the device. During image acquisition, the stepping motor drove the linear motion module to lift the drying platform out of the drying chamber. When the platform was raised to 250 mm from the 3D sensor, the 3D information image was

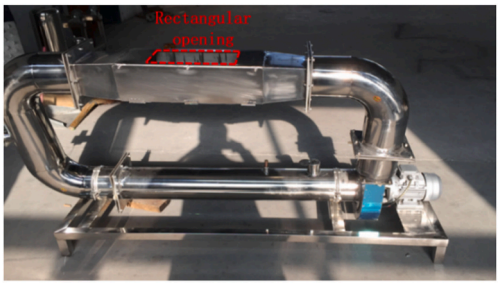

Fig. 1. Homemade tunnel hot air dryer.

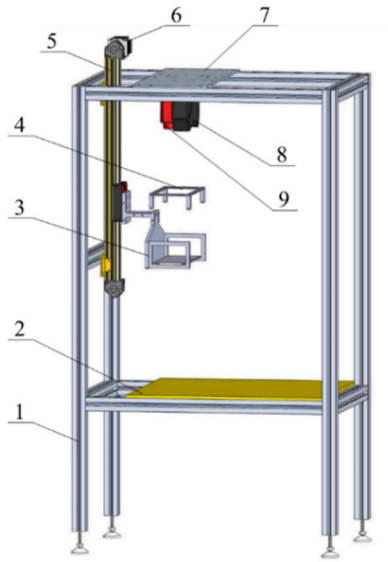

Fig. 2. Online acquisition device. The device was comprised of: 1. External framework; 2. control system board; 3. Lifting structure; 4. Drying platform; 5. Linear motion module; 6. Stepper motor; 7. Sensor fixing plate; 8.3D information sensor; 9. Temperature sensor.

acquired. After this, the drying platform returned to its original position.

2.3. Methods

After setting the parameters, the tunnel hot air dryer was started for 30 min until the drying environment was stable. Then, four slices of potato to be dried were placed in the tunnel: two were used to obtain 3D morphological information, one was used to obtain temperature field information and the remaining one was weighed during the drying process. The control system automatically lifted the potato slices out of the drying chamber of the dryer every 5 min and the information acquisition module acquired the current 3D morphological and temperature field information of the potato slices. At the same time, the potato slice for weighing was removed from the drying platform and returned after the weighing was completed. When the weight of the potato slice no longer changed, the tunnel hot air dryer was switched off and drying was terminated.

As shown in Table 1, the influential factors that were explored in this study were humidity, temperature, velocity, slice diameter and slice thickness, with three levels for each factor in the drying experiments. Three replicate experiments were required for each level. In the experiments, the levels of other factors that were not part of the current test factors were defaulted to fixed values (hot air humidity 20% RH, hot air temperature 70 °C, hot air velocity 5 m/s, slice diameter 35 mm, slice thickness 4 mm).

2.4. Image processing

To study the correlation between the 3D morphology of potato slices and the temperature distribution in potato slices during the drying process, the images acquired by the sensors were first processed and the 3D information and temperature information were obtained. The image processing flow is shown in Fig. 3.

Table 1
Experimental design for correlation study.

Influential factors	Levels		
	1	2	3
Hot air humidity (%RH)	10	20	30
Hot air temperature (°C)	60	70	80
Hot air velocity (m/s)	3	5	7
Slice diameter (mm)	25	30	35
Slice thickness (mm)	2	4	6

2.4.1. 3D information image processing

The 3D morphological data acquired by the 3D information sensor was output as an image in 16-bit RGB format. The 16-bit grey-scale image, termed the height image, containing the height information of the potato slices, was obtained by extracting the data from channel B. Its grey value was linearly related to the Z axis value of the actual coordinates. Thus, after processing, the 3D information from each potato slice was translated into 2D grey-scale images for processing. The processing mainly consisted of region of interest (ROI) extraction and conversion of point cloud data.

As shown in Fig. 4, the ROI was extracted by threshold segmentation, hole filling and morphological erosion. Threshold segmentation aimed to remove the background of the image. During data acquisition, the height of the drying platform was fixed, so the grey value distribution of the background in the image remained constant. Threshold segmentation was performed by setting a global threshold. The grey value at the bottom of the valley between the two peaks of the grey distribution histogram was taken as the threshold T, and the value of T was 36000.

Due to the reflection of residual moisture on the surface of the potato slices, there were holes in the images with missing pixel data. These holes needed to be filled. These holes were filled by calculating the average grey value of the pixels within the specified grey value range of the adjacent window of the holes. The window was a rectangular window of 5 × 5 pixels, and the specified range of the grey-scale values was 36000–42000. In addition to the holes in the images, some of the potato slice images had some mixed pixels at the edges that needed to be removed. The morphological erosion operation was used to remove the mixed pixels at the edges of the images. The structure element for the erosion operation was a circle with a radius of 3.5. Fig. 4 presents images of potato slices after erosion.

After the ROI was extracted, the pixel coordinates (P_x, P_y, P_z) of the height image could be converted into actual 3D coordinates (X, Y, Z) using Equation (1).

$$\begin{bmatrix} X \\ Y \\ Z \end{bmatrix} = \begin{bmatrix} P_x \\ P_y \\ P_z \end{bmatrix} \begin{bmatrix} X_{REZ} & Y_{REZ} & Z_{REZ} \end{bmatrix} + \begin{bmatrix} X_{offset} \\ Y_{offset} \\ Z_{offset} \end{bmatrix} \quad (1)$$

where X_{REZ}, Y_{REZ} and Z_{REZ} are the resolution of the coordinate axis, and X_{offset}, Y_{offset} and Z_{offset} are the offset of the coordinate axis.

2.4.2. Temperature information image processing

The temperature field information acquired by the infrared thermal imaging sensor was output in the form of a single-channel 16-bit grey-scale image. The temperature information image reflected the temperature distribution of the potato slice and its surrounding drying platform. The larger the grey value of the image, the higher the temperature.

The processing of temperature information images consisted of extraction of the ROI and conversion of actual temperature values. The first column of Fig. 5 presents a set of temperature information images acquired at the early (0 min), middle (60 min) and late (120 min) stages of experimental drying. The images exhibited obvious edge features, but the edges were blurred and were considered weak edges. Thus, Sobel edge detection was chosen to detect and convert the images into edge images, as shown in the second column of Fig. 5. The edge images were divided into multiple connected domains using maximum between-class variance method (OTSU) as a threshold segmentation algorithm. The ROI was obtained by screening the area of connected domains. The segmentation results of the potato slices are shown in the third column of Fig. 5.

The temperature information images acquired in the experiment

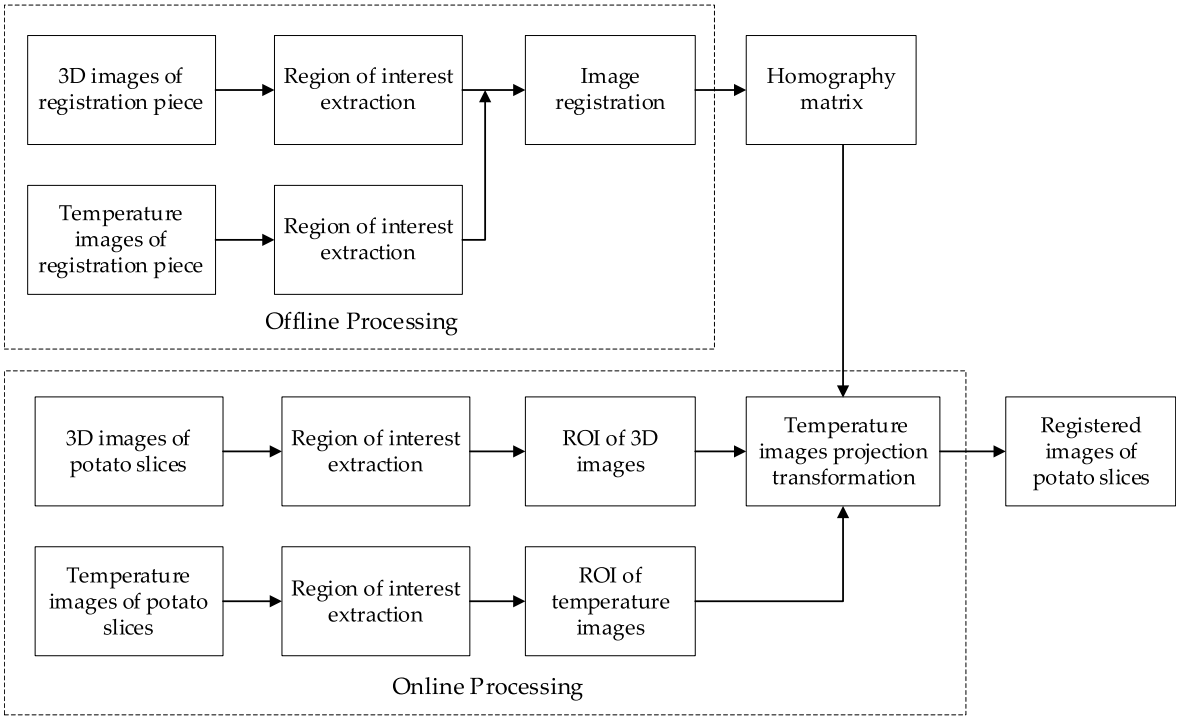

Fig. 3. Image processing flow.

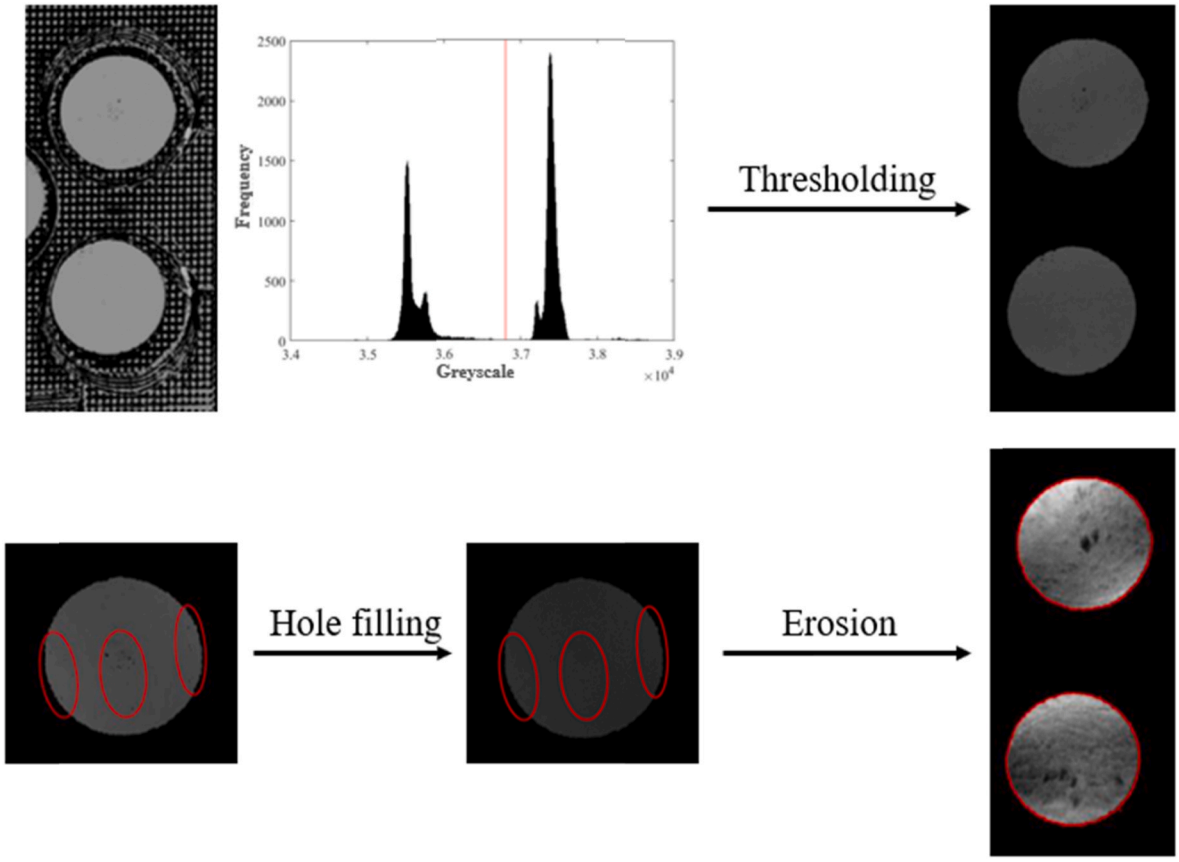

Fig. 4. 3D information image processing. The processing included threshold segmentation, hole filling and morphological erosion.

were 16-bit grey-scale images, and the image data needed to be converted. According to Equation (2), the grey value of each pixel was converted to the corresponding actual temperature value.

$$T = 0.4G - 273.15 \quad (2)$$

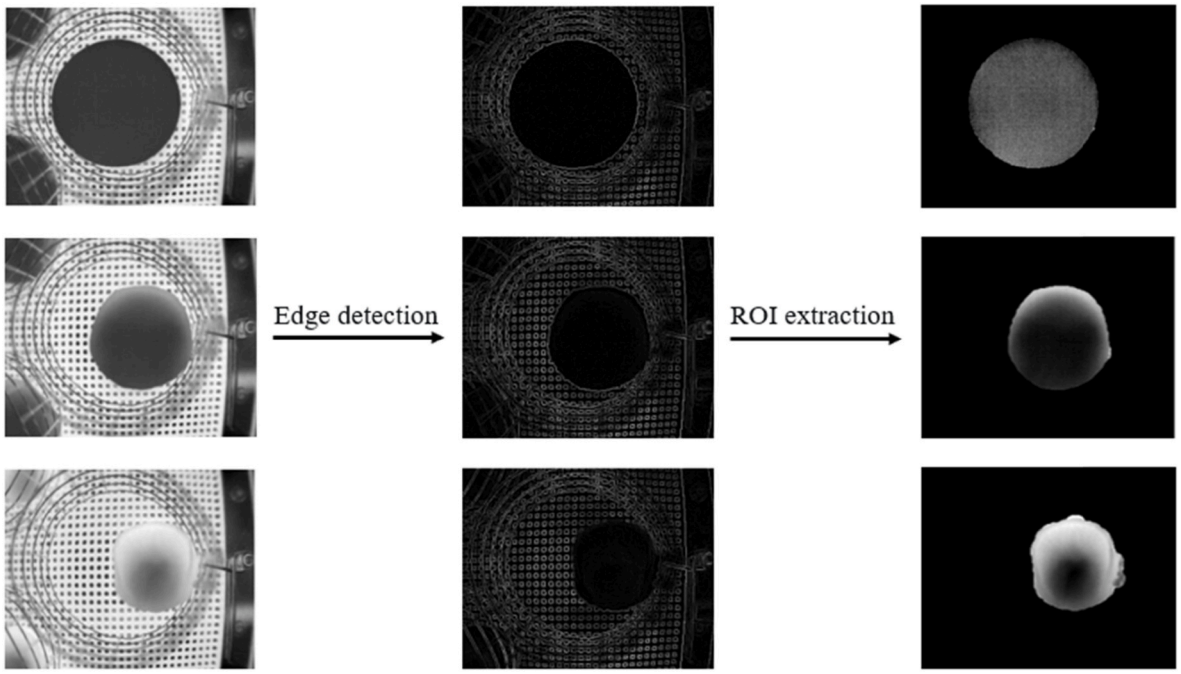

Fig. 5. Temperature images, edge images and ROI extraction results of each drying stage. Each column shows images from top to bottom at 0 min, 60min and 120 min. The first column is temperature images, the second column is edge images and the third column is ROI extraction results.

where T is the actual temperature value and G is the grey value of the temperature image.

2.4.3. Methods of image registration

3D images and temperature images were captured using a 3D sensor and temperature sensor, respectively; however, due to the different spatial locations, resolutions and sizes of the two sensors, the two acquired images needed to be registered so that the local optimum of the source image (temperature image) could be mapped to the target image (3D image). This allowed for better analysis of the 3D information corresponding to the temperature information.

There are two main types of image registration algorithms: grey-scale-based registration and feature-based registration. The grey-scale values of the potato slice regions on the 3D images and the temperature images had different meanings; they did not have similar grey-scale features. Therefore, the feature-based registration method was chosen for this study. The registration process is shown in Fig. 6.

At the same time, the potato slices themselves were flat on the top surface and were a regular round shape; thus, they contained too few feature points to facilitate image feature point detection and post-registration. In order to increase the number of feature points in each image, a registration piece (Fig. 7) was designed in this study using black acrylic as the material. This was used for the pre-registration of the two sensor images. The results were applied to the post-registration of the 3D and temperature information of the potato slices. The registration piece was designed as a cylinder with a thickness of 4 mm and a diameter of 35 mm.

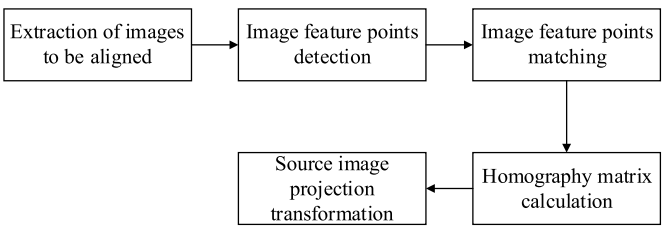

Fig. 6. Registration process design.

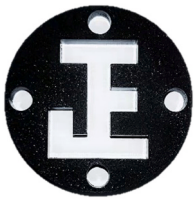

Fig. 7. Registration piece design.

The registration piece was placed on the drying platform. 3D images and temperature images of the registration piece were acquired, and the ROI was extracted from the acquired images. The Scale Invariant Feature Transformation (SIFT) algorithm was chosen to detect the feature points. Then, the feature description of feature points was created.

The random sample consensus (RANSAC) algorithm was used to match the feature points of the registration piece. A random selection of matching pairs from the available pairs was used to fit the projection transformation matrix. This matrix was applied to the remaining matching pairs for result verification. These two processes were repeated until the best matching pairs were obtained. As shown in Fig. 8,

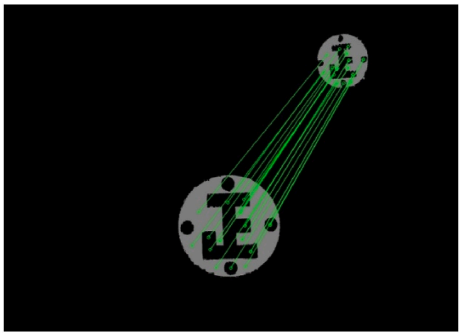

Fig. 8. Random sample consensus algorithm processing result.

21 sets of best matching pairs were ultimately obtained.

The homography matrix was calculated from the matching pairs. The matrix was brought into the projection transformation of the source image, and spatial correspondence between the pixels of the source and target images was established according to geometric constraints. Finally, the pixel values were passed, and the homogeneous coordinates of the source image pixels were transformed into the homogeneous coordinates of the target image pixels. The transformation result is shown in Fig. 9.

3. Results and discussion

3.1. Contour and isotherm analysis

Analysis of the contour and isotherm maps for the different levels of the influential factors revealed similar patterns of variation in the contours and isotherms. Therefore, the contour (Fig. 10) and isotherm (Fig. 11) maps of one experimental group were selected for analysis. The parameters for the experimental group were as follows: 20% RH hot air humidity, 70 °C hot air temperature, 5 m/s hot air velocity, 35 mm slice diameter, 4 mm slice thickness. The contour maps were drawn with pseudo-colour intervals ranging from 1 to 8 mm, with a line spacing of 0.3 mm. The isotherm maps were drawn from 20 to 70 °C, with a line spacing of 2 °C.

As can be seen in Figs. 10 and 11, the area occupied by the potato slices in the image decreased during the drying process. This indicates that the potato slices were shrinking. Shrinkage was caused by an imbalance between the internal and external pressure of the potato slices during the drying and dehydration processes. In addition, the warped position of the potato slices changed slightly at different time points, as shown in Fig. 10. This small rotation of the potato slices was caused by the blowing of the hot air. The three rows in Figs. 10 and 11 are divided into three stages, namely, the early, middle and late stages of potato drying, in order to describe the trends of variation in the contour and isotherm distributions during the drying process.

In the early stage of drying, as shown in the first row of both figures, the left and right sides of the potato slices began to warp slightly, but not significantly, and the height of the central area decreased. This was due to shrinkage in the thickness of the potato slices due to the loss of moisture, which counteracted some of the edge warpage that occurred due to stress. At the same time, the temperature field distribution of the potato slices transitioned from a homogeneous to an inhomogeneous distribution. The temperature rose rapidly in the lower area of the potato slices and also rose in the upper area of the centre, but at a slower rate. This was reflected in the gradual increase in the isotherms. As can be seen in the two figures, at this stage, warpage in the potato slices clearly occurred on either side of the higher temperature area. This was due to the higher rate of moisture loss and faster rate of shrinkage in the high-temperature area. Further, stress from the shrinkage of the slices drove warpage on both sides of the high-temperature area (Fig. 12).

In the middle stage of drying, as shown in the second row of both figures, the height of the central area of the potato slices basically stopped decreasing. The warpage on both sides became progressively more pronounced and the contour density increased. At this time, the temperature distribution range of the potato slices was further expanded, and the rate of temperature increase in the outer area was higher than that in the central area. This was reflected in the increasing density of the isotherms. The area of high temperature started to move gradually from the lower left of the earlier period to the lower right. As can be seen in the contour map, warpage was more evident on the lower right side of the potato slices. This movement was caused by the further reduction in the angle between the warpage area and the wind direction of the hot air. The angle reduction increased the efficiency of heat capture by the potato slices.

In the later stage of drying, as shown in the third row of both figures, the warpage on the sides of the potato slices was already very evident. However, the degree of change in warpage during this stage was small and the contour density did not change much. At this time, the potato slices had essentially lost all moisture within their cells. The slices hardened, and the skeleton gradually changed to a glassy state (Li et al., 2021). At this stage, the temperature of the outer area of the potato slices remained essentially constant and heat was transferred to the central area. The temperature of the central area gradually increased. The overall temperature distribution of the potato slices also tended to become progressively homogeneous, as shown by a decrease in the number of isotherms.

Overall, there was a correlation between the change in the contour and the change in the isotherm as the drying time of the potato slices changed. In order to better quantify the correlation, the correlation between the 3D information and the temperature information was investigated by examining the relationships between various parameters of height and temperature (i.e., mapping, range, average) over time for the same acquisition point.

3.2. Parameter correlation study

3.2.1. Correlation study between temperature and height

After registration, there was a bijective relationship between the 3D image pixels and the temperature image pixels (acquisition points) of the same potato slice. In order to investigate whether there was a correlation between temperature and height at the same acquisition point, an experimental group was selected as the sample group. The parameters for the experimental group were as follows: 20% RH hot air humidity, 70 °C hot air temperature, 5 m/s hot air velocity, 35 mm slice diameter, 4 mm slice thickness. Temperature-height scatter plots (Fig. 13) were plotted for all acquisition points at each acquisition time point. Areas of the plots with different scatter densities are presented in different colours.

Two types of correlation coefficients, Pearson correlation coefficients and Spearman's rank correlation coefficients, are often evaluated in

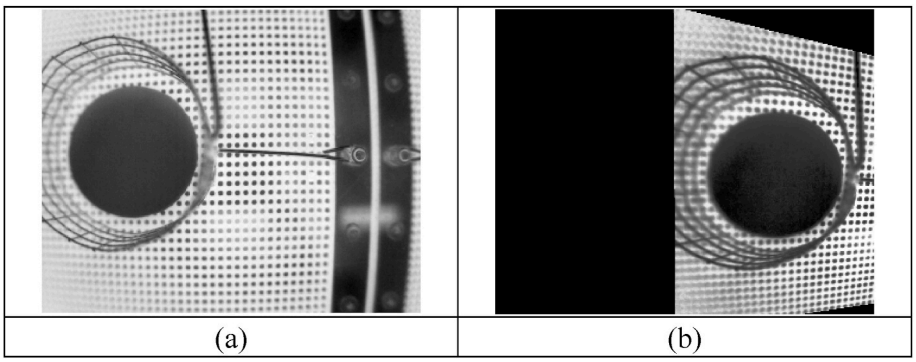

Fig. 9. Source image projective transformation result. (a) Before projective transformation; (b) after projective transformation.

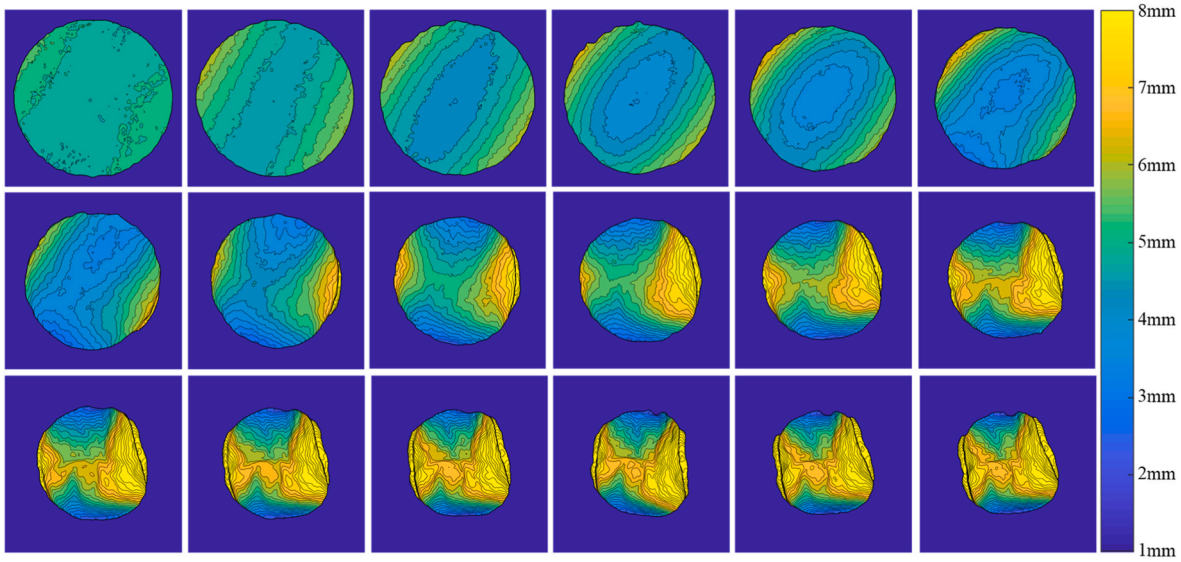

Fig. 10. Contour map.

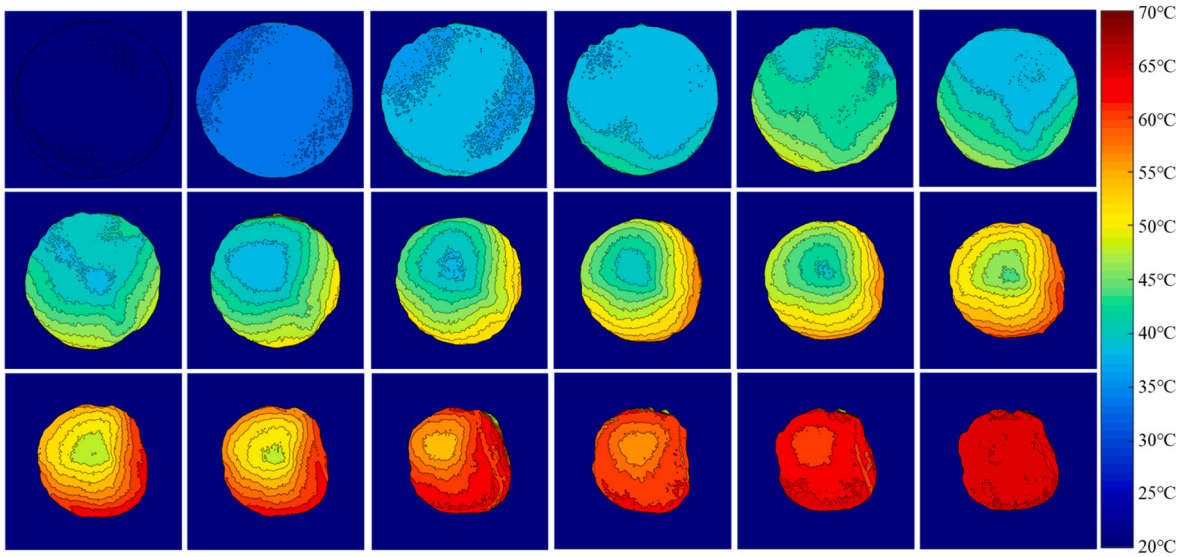

Fig. 11. Isotherm map.

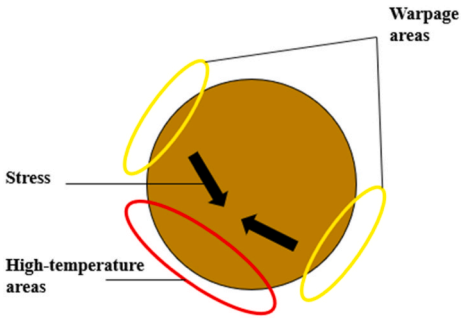

Fig. 12. Temperature change linked to warpage change.

experimental studies. Pearson correlation coefficients are generally used when there is a normal distribution between the two variables, while Spearman's rank correlation coefficients are used when there is a lack of normality in the distribution of the variables. Thus, first, each variable was examined for normality to determine the type of correlation coefficient to be used.

The data for the sample group was extracted from tens of thousands of pixels, and thus, the sample size was very large. As such, Jarque-Bera (JB) hypothesis testing was used to determine whether both temperature and height obeyed a normal distribution. First, the null hypothesis H0 and the alternative hypothesis H1 were as follows.

H0. Both variables obey a normal distribution.

H1. Both variables do not obey a normal distribution.

The JB testing for the two variables at each acquisition time point revealed that the confidence levels for the normal distribution tests were under 95%.

The results of the normal distribution tests (Table 2) indicated that the h values for both variables were 1 and the p values were less than 0.05. Therefore, the null hypothesis was rejected, and the alternative hypothesis was accepted. That is, both variables were not normally distributed. Therefore, Spearman's rank correlation coefficients were used for the correlation analyses in this study.

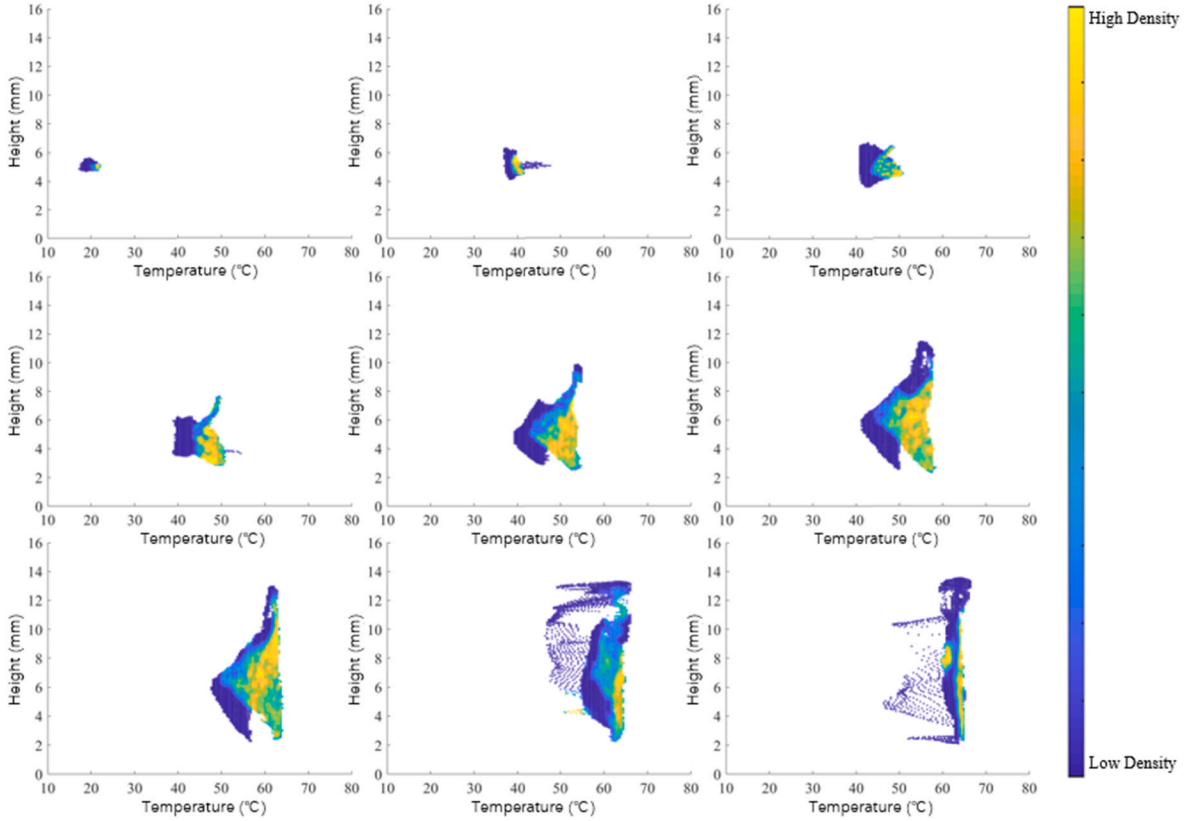

Fig. 13. Temperature-height scatter plots at different acquisition time points.

Table 2
Results of the normal distribution tests for the sample group temperature-height data.

Acquisition time point	Temperature		Height	
	h	p	h	p
0 min	1	<0.001	1	<0.001
5 min	1	<0.001	1	<0.001
10 min	1	<0.001	1	<0.001
15 min	1	<0.001	1	<0.001
20 min	1	<0.001	1	<0.001
25 min	1	<0.001	1	<0.001
30 min	1	<0.001	1	<0.001
35 min	1	<0.001	1	<0.001
40 min	1	<0.001	1	<0.001
45 min	1	<0.001	1	<0.001
50 min	1	<0.001	1	<0.001
55 min	1	<0.001	1	<0.001
60 min	1	<0.001	1	<0.001
65 min	1	<0.001	1	<0.001
70 min	1	<0.001	1	<0.001
75 min	1	<0.001	1	<0.001
80 min	1	<0.001	1	<0.001
85 min	1	<0.001	1	<0.001

Table 3
Spearman's rank correlation coefficients and MICs for the temperature-height data.

Acquisition time point	Spearman's rank correlation coefficient	MIC
0 min	0.0600	0.0774
5 min	−0.7733	0.4738
10 min	−0.5408	0.3221
15 min	−0.0878	0.2104
20 min	0.0298	0.1902
25 min	−0.1312	0.1490
30 min	0.1163	0.2481
35 min	0.2065	0.2812
40 min	0.2205	0.2529
45 min	0.2680	0.3007
50 min	0.0880	0.2392
55 min	0.1061	0.2634
60 min	0.1848	0.2711
65 min	0.1977	0.2750
70 min	0.1197	0.1374
75 min	0.0493	0.2148
80 min	−0.0832	0.1668
85 min	−0.1945	0.1846

However, the types of correlation were not observed obviously in the scatter plots. The possibility existed that the two variables did not fit a simple functional model. Thus, the Maximum Information Coefficient (MIC) was also calculated and compared with the Spearman's rank correlation coefficients.

Compared to Spearman's rank correlation coefficients, MIC values provide a better response to correlations between variables that are consistent with a complex model.

As can be seen from Table 3, the absolute values of the Spearman's rank correlation coefficients for the temperature and height scatter distributions at the same acquisition point were basically around 0.1 and the MICs were all around 0.2. Thus, it can be concluded that there was essentially no strong correlation between temperature and height in this study. Therefore, there will be no further analysis or discussion of these parameters in this paper.

3.2.2. *Correlation study between the range of temperature and height*

Variations in the range of the height and temperature data could reflect changes in height and temperature gradients during the drying of each potato slice. To examine the correlation between these parameters over time, the same sample group as above was selected for analysis. The maximum and minimum temperature and height values for this group of

potato slices during drying are shown in Fig. 14. This figure shows the changes in the temperature range and height range.

The Spearman's rank correlation coefficient and MIC for the temperature range and height range were calculated to be 0.3604 and 0.7359, respectively. This suggests that the temperature range data did not correlate with the height range data in a simple functional model, but there was a strong correlation in a complex functional model.

3.2.3. Correlation study between the average temperature and height

Variations in the average height and temperature data could reflect the overall change in the height and temperature during the drying of a potato slice. To examine the correlation between these parameters over time, the same sample group as above was selected for analysis. The variation in the average temperature and height during the drying process of this group of potato slices is shown in Fig. 15.

The Spearman's rank correlation coefficient and MIC for the average temperature and height were calculated to be 0.8962 and 0.9986, respectively. The average temperature and height values exhibited an extremely strong correlation.

3.2.4. Results of the correlation study

The above results indicated that the correlation between height and temperature was better described by the averages of the temperature data and height data, respectively. Thus, Spearman's rank correlation coefficients and MICs (Table 4) for these parameters were calculated for each experimental variable and level. As can be seen from Table 4, the Spearman's rank correlation coefficients were mostly above 0.7 in absolute value and the MICs were mostly above 0.9.

In summary, both the Spearman's rank correlation coefficients and MIC values revealed strong or extremely strong correlations between the averages of the temperature data and height data. This indicates that there is a correlation between the overall trend in the 3D morphology and changes in the temperature information during the drying of potato slices.

The morphological change pattern of the drying process obtained in this paper was similar to the results of the drying models reported by Jiao (2022) and Li (2022) for hot air-dried potato and bamboo shoot slices, respectively. Furthermore, Jiao and Li found that the drying model was a good predictor of the temperature distribution within the potato and bamboo shoot slices at different time periods and the shrinkage during drying. However, they only investigated volume shrinkage vs. moisture ratio and temperature distribution vs. moisture ratio during drying, and did not explore the relationship between temperature distribution and shrinkage in depth. In this paper, the correlation between the two was explored to directly quantify the relationship between them. This provided a new and more intuitive strategy for studying the 3D morphological changes during material drying.

Despite the exciting results obtained, the research process of this paper still had some flaws. The samples used for the study were round potato slices to facilitate observation and comparison of the 3D morphological changes during drying. However, this ignored the effect of sample shape on drying shrinkage. Shrinkage of potato slices during hot air-drying is anisotropic (Jiao, 2022). The regular round structure will weaken this effect, resulting in some deviation of the sample shrinkage from the actual scene. Therefore, the investigation of potato slice shrinkage in other geometries will be the next study in this paper.

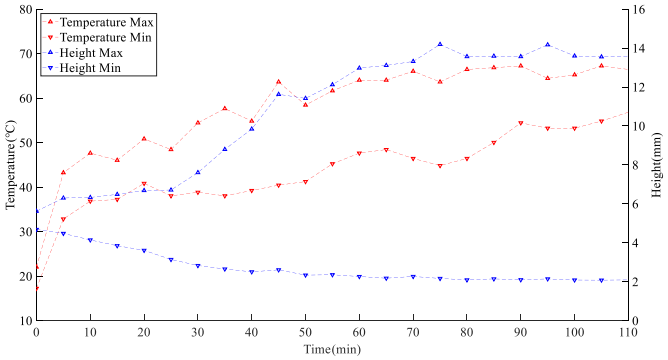

Fig. 14. Temperature/height Max & Min vs time.

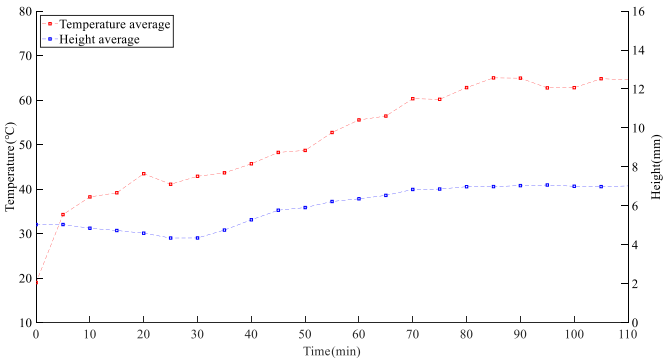

Fig. 15. Temperature/height average vs time.

Table 4
Spearman's rank correlation coefficients and MICs of the different variables and levels.

Variable	Level	Spearman's rank correlation coefficient	MIC
Hot air humidity (% RH)	10	0.6351	0.9984
	20	0.8962	0.9986
	30	0.3354	0.7785
Hot air temperature (°C)	60	0.7108	0.9427
	70	0.8962	0.9986
	80	0.7857	0.9984
Hot air velocity (m/s)	3	0.6825	0.9183
	5	0.8962	0.9986
	7	0.7737	0.7512
Slice diameter (mm)	25	−0.0684	0.3052
	30	−0.1948	0.9984
	35	0.8962	0.9986
Slice thickness (mm)	2	0.7055	1.0000
	4	0.8962	0.9986
	6	−0.3571	0.9990

4. Conclusions

In this study, 3D information images and temperature information images of potato slices were registered using the RANSAC algorithm. Correlation analyses were conducted on the 3D information and temperature information of the slices. Three parameters were calculated, i.e., mapping, range and average, for each acquisition point and each variable, and correlation analysis was performed to examine the relationships. Spearman's rank correlation coefficients and MICs were selected as measures for the correlation study. The results indicated that there was an extremely strong correlation between the height averages of the 3D images and the temperature averages of the temperature images. Thus, it can be concluded that there is a correlation between the overall trend in the 3D morphology and temperature information changes during the drying of potato slices. This paper gives a new approach to investigate the morphological changes in the drying process by quantifying the relationship between 3D morphology and temperature distribution. This provides an important theoretical support for studying the material shrinkage of the drying process and optimizing the drying process.

Funding

This research received no external funding.

CRediT authorship contribution statement

Li Sun: Conceptualization, Methodology, Software, Validation, Data curation, Project administration, Funding acquisition. **Xin Zheng:** Methodology, Validation, Investigation, Writing – original draft, preparation, Writing – review & editing. **Pengqi Zhang:** Investigation. **Jianrong Cai:** Conceptualization, Validation, Resources, Data curation, Visualization, Supervision. **Junwen Bai:** Conceptualization, Resources, Writing – review & editing, Visualization, Supervision.

Declaration of competing interest

The authors declare that they have no known competing financial interests or personal relationships that could have appeared to influence the work reported in this paper.

Data availability

No data was used for the research described in the article.

References

Anne-Katrin, Mahlein, Elias, Alisaac, Masri, Ali Al, et al., 2019. Comparison and combination of thermal, fluorescence, and hyperspectral imaging for monitoring Fusarium head blight of wheat on spikelet scale. Sensors 19 (10), 2281.

Bernhard, Biskup, Hanno, Scharr, Ulrich, Schurr, et al., 2007. A stereo imaging system for measuring structural parameters of plant canopies. Plant Cell Environ. 30 (10), 1299–1308.

Cai, Jianrong, Lu, Yue, Bai, Junwen, et al., 2019. Three-dimensional imaging of morphological changes of potato slices during drying. Trans. Chin. Soc. Agric. Eng. 35 (1), 278–284.

Chen, Kun, 2019. Research on the Rapeseed Data Processing Methods Based on Laser Point Cloud. Huazhong Agricultural University.

Chen, Liu, 2020. On-line Detection and Research of Three-Dimensional Shape and Temperature Field of Potato Slices Drying Process. Jiangsu University.

Cheng, Qiang, 2018. Research on Microwave Temperature Field Simulation and Energy Consumption of Microwave Vacuum Drying of Potato Slices. Harbin University of Commerce.

Cheng, Xiaohui, Lin, Li, Xiao, Shuai, et al., 2020. Problems and countermeasures of using potato as staple food. Cereals & Oils 33 (1), 12–14.

Colaizzi Paul, D., O'Shaughnessy Susan, A., Evett Steven, R., 2018. Calibration and tests of commercial wireless infrared thermometers. Appl. Eng. Agric. 34 (4), 647–658.

Gao, Kun, Tian, Xiaohong, Tan, Bin, et al., 2021. Current situation and prospect of potato food processing research and development. J Chinese Cereals Oils Assoc 36 (8), 161–168.

George, Azzari, Rusu, Radu B., Goulden, Michael L., 2013. Rapid characterization of vegetation structure with a microsoft kinect sensor. Sensors 13 (2), 2384–2398.

Huang, Fengling, Zhang, Lin, Li, Xiande, et al., 2017. Development situation and countermeasures of China's potato industry. Agric. Outlook 13 (1), 25–31.

Jiang, Xin, Yin, Wenqing, Pu, Hao, et al., 2019. Measurement method of grain volume on screw conveyor based on structured light of 3D vision. J. Nanjing Agric. Univ. 42 (2), 373–381.

Jiao, Junhua, 2022. Experimental Study and Numerical Simulation of Hot Air Drying Process of Potato. Zhengzhou University of Light Industry.

Kelkar, Shivangi, Scott, Stella, Boushey, Carol, et al., 2011. Developing novel 3D measurement techniques and prediction method for food density determination. Procedia Food Sci 1, 483–491.

Khan Hammad, A., Nakamura, Yukiko, Furbank Robert, T., et al., 2021. Effect of leaf temperature on the estimation of photosynthetic and other traits of wheat leaves from hyperspectral reflectance. J. Exp. Bot. 72 (4), 1271–1281.

Li, Zichun, 2022. Study on Hot Air Drying Characteristics and Heat and Moisture Migration Pattern of Bamboo Shoot Slices. Shandong Jianzhu University.

Li, Yaqi, Zhang, Pengqi, Cai, Jianrong, et al., 2021. Analysis of warpage variations in potato slices during hot air drying. Food Sci. (N. Y.) 42 (23), 123–128.

Liu, Jing, 2021. General situation of potato planting and measures to improve benefits in China. Agric. Eng. 11 (10), 142–144.

Liu, Yu, Liu, Sa, Yang, Changhui, et al., 2020. Three-dimensional spatial localization of overlapping citrus based on binocular stereo vision. J. Agric. Sci. Technol. 22 (9), 104–112.

Luo, Qiyou, Liu, Yang, Gao, Mingjie, et al., 2015. Status Quo and prospect of China's potato industry. Agric. Outlook 11 (3), 35–40.

Mahiuddin, Md, Md Imran, H., Khan, Kumar, C., et al., 2018. Shrinkage of food materials during drying: current status and challenges. Compr. Rev. Food Sci. Food Saf. 17 (5), 1113–1126.

Makhsous, Sepehr, Mohammad, Hashem M., Schenk, Jeannette M., et al., 2019. A novel mobile structured light system in food 3D reconstruction and volume estimation. Sensors 19 (3), 564.

Moore Caitlin, E., Meacham-Hensold, Katherine, Pauline, Lemonnier, et al., 2021. The effect of increasing temperature on crop photosynthesis: from enzymes to ecosystems. J. Exp. Bot. 72 (8), 2822–2844.

Sun, Li, Zhang, Pengqi, Zheng, Xin, et al., 2021. Three-dimensional morphological changes of potato slices during the drying process. Curr. Res. Food Sci. 4, 910–916.

Wang, Qionghua, Wang, Aihong, 2010. Survey on stereoscopic three-dimensional display. J. Comput. Appl. 30 (3), 579–581+588.

Wang, Heng, Cao, Shukun, Cui, Yi, et al., 2018. Analysis of temperature field of grain and drying medium for grain drying integrated mechanical device. MATEC Web of Conferences 175 (3), 20–24.

Wang, Chuanxu, Wang, Kang, Lin, Chen, et al., 2021. Research and realization of granary temperature field prediction model based on kriging interpolation and BP neural network. J. Agric. Sci. Technol. 23 (9), 96–102.

Xi, Feng, Hu, Qiaoqun, Zhu, Aishi, 2018. Model and character of hot air convection drying of potato slice. Cereals & Oils 31 (7), 52–55.

Xu, Chao, Zhao, Yaqi, Wang, Qing, et al., 2022. Shelf quality changes of fresh-cut potatoes during storage. Food Ferment. Ind. 1–11.

Yang, Pengshu, Liu, Hui, Wang, Xiaocui, et al., 2021. Three-dimensional information detection method for crop seedling obstacles based on binocular vision. J Agri Mechanization Res 43 (4), 11–16.

Zhang, Shuo, 2021. Research on Potato Planting Regionalization in China. Chinese Academy of Agricultural Sciences.

Zheng, Lihua, Mai, Chunyan, Liao, Wei, et al., 2016. 3D point cloud registration for apple tree based on Kinect camera. Trans. Chin. Soc. Agric. Mach. 47 (5), 9–14.